PHYSICAL REVIEW D **92,** 054506 (2015)

Hadronic vacuum polarization and muon $g-2$ from magnetic susceptibilities on the lattice

Gunnar S. Bali[1,2] and Gergely Endrődi[1,*]

[1]*Institute for Theoretical Physics, Universität Regensburg, D-93040 Regensburg, Germany*
[2]*Department of Theoretical Physics, Tata Institute of Fundamental Research, Homi Bhabha Road, Mumbai 400005, India*

(Received 6 July 2015; published 21 September 2015)

We present and test a new method to compute the hadronic vacuum polarization function in lattice simulations. This can then be used, e.g., to determine the leading hadronic contribution to the anomalous magnetic moment of the muon. The method is based on computing susceptibilities with respect to external electromagnetic plane wave fields and allows for a precision determination of both the connected and the disconnected contributions to the vacuum polarization. We demonstrate that the statistical errors obtained with our method are much smaller than those quoted in previous lattice studies, primarily due to a very effective suppression of the errors of the disconnected terms. These turn out to vanish within small errors, enabling us to quote an upper limit. We also comment on the accuracy of the vacuum polarization function determined from present experimental R-ratio data.

DOI: 10.1103/PhysRevD.92.054506 PACS numbers: 12.38.Gc, 12.38.Mh, 25.75.Ag, 25.75.Ld

I. INTRODUCTION

The most precise measurement of the anomalous magnetic moment of the muon, obtained by E821 at Brookhaven [1], differs by more than three standard deviations from the theoretical expectation. At present, the uncertainties on the theory and on the experimental sides are of similar sizes. For recent reviews and analyses, see, e.g., Refs. [2–6]. With the planned E989 experiment at Fermilab [2] and E34 at J-PARC [7], it is of utmost importance to increase the precision of the standard model prediction in line with the expected experimental improvement by a factor of about five [1,2,7]. If the discrepancy persisted at this even higher level of accuracy, this should help to pin down any particular beyond-the-standard-model scenario and constrain the parameters of new interactions. With an impressive QED five-loop evaluation [8] available, the theoretical uncertainty is dominated by nonperturbative effects and, in particular, by the leading hadronic contribution to the electromagnetic vacuum polarization tensor, with the second biggest source of uncertainty being the hadronic light-by-light scattering contribution. The hadronic contribution to the vacuum polarization tensor is also important in view of the running of the electromagnetic fine-structure constant and of the Weinberg weak mixing angle [4,9–12] from low to high scales.

The standard method [13,14] employed in lattice calculations of the leading hadronic contribution to the anomalous magnetic moment $a_\ell = (g_\ell - 2)/2$ of a charged lepton $\ell \in \{e, \mu, \tau\}$ consists of computing the renormalized vacuum polarization function and inserting this into the leading-order QED formula. The hadronic vacuum polarization tensor, which is the main object of this study, is defined as

$$\Pi_{\mu\nu}(p) = \int \mathrm{d}^4x e^{ipx} \langle j_\mu(x) j_\nu(0) \rangle = (p_\mu p_\nu - \delta_{\mu\nu} p^2)\Pi(p^2), \tag{1}$$

where

$$j_\mu = \frac{q_u}{e}\bar{u}\gamma_\mu u + \frac{q_d}{e}\bar{d}\gamma_\mu d + \frac{q_s}{e}\bar{s}\gamma_\mu s + \cdots \tag{2}$$

denotes the quark electromagnetic current in position space and $q_u/e = 2/3$, $q_d/e = q_s/e = -1/3$ are the fractional quark charges. Due to electromagnetic current conservation, $\Pi_{\mu\nu}$ is transverse and can be parametrized in terms of a single vacuum polarization function $\Pi(p^2)$, where we employ Euclidean spacetime conventions, i.e. the spacelike $p^2 > 0$ correspond to virtualities. $\Pi(p^2)$ undergoes additive renormalization but the renormalized combination

$$\Pi_{\mathrm{R}}(p^2) = \Pi(p^2) - \Pi(0) \tag{3}$$

is ultraviolet finite.

It turns out that the leading hadronic contribution $a_\mu^{\mathrm{had,LO}}$ to the anomalous magnetic moment of the muon [see the definition equation (4) below] depends most strongly on $\Pi_{\mathrm{R}}(p^2)$ at relatively small argument values. Since small momenta correspond to large Euclidean distances, naively implementing Eq. (1) results in a bad signal over noise ratio in this region. This becomes even worse for calculations of the quark-line disconnected contributions, which therefore have been neglected in almost all previous lattice studies. Where these were taken into account [15–17], they

*Corresponding author.
gergely.endrodi@physik.uni-r.de.

dominated the statistical error. Another problem of many past lattice attempts is a conceptual one: $\Pi(0)$ often is extrapolated from $\Pi(p^2)$ at $p^2 > 0$ and the parametrization used constitutes a source of systematic uncertainty that is difficult to estimate.

Here we propose methods that address both of the above issues. The vacuum polarization at $p^2 = 0$ is shown to be equal to the bare magnetic susceptibility of the system, which can be determined independently on the lattice. We investigate different methods to achieve this, giving consistent results. We also discuss how this quantity diverges as a function of the lattice spacing towards the continuum limit.

Most importantly, we introduce a new method for computing both the connected and the disconnected contributions to the hadronic vacuum polarization function with unprecedented precision, in particular at small momenta. This consists of calculating $\Pi(p^2)$ at $p^2 > 0$ through the response of the system to oscillatory background electromagnetic fields. The new method is similar in spirit to employing momentum sources [18,19], allowing us to spend more effort on the low-p^2 points, thereby increasing their precision, without wasting resources on large momenta where $\Pi_{\rm R}(p^2)$ can easily be obtained within small relative errors, with a much smaller impact on the predicted value of $a_\mu^{\rm had,LO}$.

The methods are tested on $N_f = 2 + 1$ staggered ensembles at the physical point, neglecting QED effects on the quark propagation which are of a higher order in the fine-structure constant α. In this situation, due to $\sum_{f\in\{u,d,s\}} q_f = 0$, disconnected contributions vanish for $m_s = m_{ud}$ but need to be taken into account for $m_s > m_{ud}$, which we do. Since we neglect charm quark effects, we have to restrict ourselves to $p^2 < m_c^2$. At high momenta our results can, however, be combined with measurements of the R ratio as well as with perturbation theory: the nonsinglet and singlet QCD contributions to the Adler function have been calculated in massless QCD to $\mathcal{O}(\alpha_s^4)$ in the strong coupling constant in Refs. [20–21], respectively.

This article is organized as follows. In Sec. II we review previous calculational strategies, followed by Sec. III, where we introduce our background field method and link this to magnetic susceptibilities. We also discuss renormalization issues and comment on relations between the Adler function and the entropy density at high temperatures. Finally, in Sec. IV we present the simulation setup and first results, before we conclude. The equivalence between magnetic susceptibilities and the vacuum polarization is demonstrated in Appendix A, and the details of our numerical implementation are discussed in Appendixes B–C.

II. SUMMARY OF PREVIOUSLY EMPLOYED METHODS

The leading hadronic contribution to the anomalous magnetic moment is given as [13,22]

$$a_\ell^{\rm had,LO} = 4\alpha^2 \int_0^\infty {\rm d}p^2 K_\ell(p^2)\Pi_{\rm R}(p^2), \tag{4}$$

where the perturbative kernel function is defined as

$$K_\ell(p^2) = \frac{m_\ell^2 p^2 Z_\ell(p^2)^3[1 - p^2 Z_\ell(p^2)]}{1 + m_\ell^2 p^2 Z(p^2)^2} \tag{5}$$

with

$$Z_\ell(p^2) = \frac{\sqrt{1 + 4m_\ell^2/p^2} - 1}{2m_\ell^2}. \tag{6}$$

The renormalized hadronic vacuum polarization function is defined in Eqs. (1) and (3) above. Note that the above expressions are valid to leading order in terms of the QED fine-structure constant $\alpha = e^2/(4\pi) \approx 1/137$, i.e. to $\mathcal{O}(\alpha^2)$, which, at this order, can be pulled out of the integral.

In the limit of small momenta, where $\Pi_{\rm R}(p^2) \propto p^2$, the argument of the integral has its maximum at $p_0^2 \approx (\sqrt{5}–2)m_\ell^2$. For the muon with $m_\mu \approx 0.105$ GeV this implies $p_0^2 \approx 0.0026$ GeV^2: an enormous volume would be necessary to resolve this momentum region, at least without the use of twisted boundary conditions [23,24], since $\pi/p_0 \approx 2\pi/m_\mu \approx 12$ fm. Fortunately, the integral as a whole turns out to be dominated by somewhat higher momenta: it still picks up about 50% of its value from momenta larger than $10p_0^2$. The predicted value of $a_\mu^{\rm had,LO}$ strongly depends on $\Pi_{\rm R}(p^2)$ at these still relatively small momenta $p^2 \sim 0.03$ GeV^2. This is nicely illustrated, e.g., in Ref. [25], in Fig. 3 of Ref. [24] and in Fig. 1 of Ref. [17].

A. Information from experiment

The hadronic polarization tensor (and also the leading hadronic contribution to the lepton anomalous magnetic moments [22]) can be obtained by analytic continuation of the R ratio of the total cross section $\sigma(e^+e^- \to \text{hadrons})$ over the tree-level $e^+e^- \to \mu^+\mu^-$ expectation (see, e.g., Refs. [26,27]):

$$\Pi_{\rm R}(p^2) = \frac{p^2}{12\pi^2} \int_{4m_\pi^2}^\infty {\rm d}s \frac{R(s)}{s(s + p^2)}. \tag{7}$$

R-ratio measurements [4,5] can in principle be augmented by other experimental data, including τ-decays into final states containing $\pi^+\pi^-$; see, e.g., Ref. [28].

In Fig. 1 we show the so-determined renormalized vacuum polarization as a function of p^2 [29]. The present relative precision of $\Pi_{\rm R}$ is 0.64% at $p^2 = 0.025$ GeV^2, increasing to 0.74% at $p^2 = 0.6$ GeV^2 [5,29]. Achieving a statistical error below 1% around $p^2 = 0.03$ GeV^2 already constitutes an enormous challenge for present-day lattice determinations, and such results still need to be

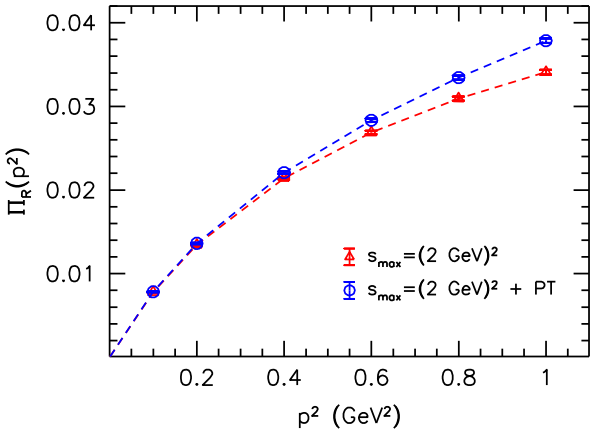

FIG. 1 (color online). The renormalized vacuum polarization determined from the experimental R ratio [29], performing the integral (7) up to $s = s_{\max} = (2\ \mathrm{GeV})^2$, where three quark flavors are active. Also indicated is the result of the integral supplemented by three-flavor perturbation theory for $s > (2\ \mathrm{GeV})^2$.

extrapolated to the infinite volume and continuum limits and, often, to physical quark masses. In principle, lattice data at large p^2 values—where discretization errors are enhanced—can be substituted by results from the R ratio. Such a combined strategy may prove optimal for an accurate determination of $a_\mu^{\mathrm{had,LO}}$, once sufficiently precise lattice results become available.

B. Lattice determinations of $\Pi(\mathbf{0})$

In the past, two strategies have been used to obtain the zero-momentum subtraction $\Pi(0)$. One possibility are fits of $\Pi(p^2)$ data, e.g., to pole parametrizations, assuming vector dominance [14,24,30–32], which is also suggested to be the dominant contribution by chiral perturbation theory [30]. Extending the fit region towards large momenta, such pole *Ansätze* have also been combined with polynomial parametrizations [15,17,30,33], motivated by perturbation theory. Another popular and less model-dependent way to obtain the normalization is through Padé approximants [24,25,34,35].

As an alternative, one can compute derivatives of $\Pi_{\mu\nu}(p)$ from its definition in terms of the continuum Fourier transformation (1). Then the divergent contribution that needs to be subtracted from $\Pi(p^2)$ can, e.g., be obtained via

$$\Pi(0) = -\frac{1}{2}\frac{\partial^2}{\partial p_\mu^2}\Pi_{\nu\nu}(p)\Big|_{p=0} \qquad (\mu \neq \nu)$$
$$= \frac{1}{2}\int \mathrm{d}^4x x_\mu^2 \langle j_\nu(x) j_\nu(0)\rangle = \frac{1}{2}\int \mathrm{d}t t^2 G(t), \quad (8)$$

where no summation over ν is implied and in the last step we identified μ with the time direction, to emphasize the correspondence to the second t-moment of a zero-momentum projected two-point function

$$G(t) = \int \mathrm{d}^3 r \langle j_i(\mathbf{r}, t) j_i(0)\rangle. \quad (9)$$

This method was used, e.g., in Refs. [36,37], to obtain this subtraction.

Finally, in Ref. [38] the expansion of the two-point current-current correlation function in powers of p_μ is carried out already on the level of quark propagators. This enables the direct computation of $\Pi(0) = \partial^2\Pi_{12}/(\partial p_1 \partial p_2)|_{p=0}$, without relying on a continuum formula. However, this comes at the price of computing the expectation value of an operator involving up to four fermion matrix inversions, without even considering disconnected contributions.

C. Lattice determinations of $\Pi(p^2)$, $\Pi_{\mathrm{R}}(p^2)$ or moments thereof

The lattice vector Ward-Takahashi identity reads $\hat{p}_\mu \Pi_{\mu\nu} = 0$ and therefore [13,14,39]

$$\Pi_{\mu\nu}(p^2) = (\hat{p}_\mu \hat{p}_\nu - \delta_{\mu\nu}\hat{p}^2)\Pi(p^2), \quad (10)$$

where $\hat{p}_\mu = (2/a)\sin(a p_\mu/2)$. This change that affects $\Pi(p^2)$ at high momenta has been implemented in almost all lattice studies, as well as a modified phase $e^{ipx} \mapsto e^{ip(x+a\hat{\mu}/2-a\hat{\nu}/2)}$ within the Fourier sum for $\mu \neq \nu$.

Most lattice evaluations use what we refer to below as the conventional method. This amounts to directly computing the lattice version of Eq. (1); see, e.g., Refs. [13–15,30–33,37]. In some cases, lower momenta were made accessible by the use of twisted boundary conditions [24,40,41]. Very recently, another interesting method, stochastically averaging over different twists, has been suggested [42] that reduces finite-volume effects and allows us to realize very small momenta. The main problem of modifying the fermionic boundary conditions is that this cannot easily be extended to incorporate quark-line disconnected contributions.

Obviously, Eq. (4) can be Taylor expanded in powers of p^2 and the coefficients can be related to those of the corresponding expansion of $\Pi_{\mathrm{R}}(p^2)$. Generalizing Eq. (8) above, the first and higher order derivatives of $\Pi_{\mu\mu}$ with respect to p^2 can be obtained, computing t^2-moments of two-point zero-momentum (spatial) projected current-current correlators. This was explored within Ref. [43] and carried out for the first few moments of the connected strange and charm quark contributions to $a_\mu^{\mathrm{had,LO}}$ in Ref. [44]. In Ref. [27] the anomalous magnetic moment was directly related to the zero-momentum projected current-current two-point function. This approach was then employed, e.g., in Refs. [16,36,41].

So far, disconnected contributions have been included in very few lattice studies [15–17]. While their effect seems to be small, the associated statistical error exceeds that of the

connected terms. Here we will find that this need not be the case. There exist theoretical expectations regarding the size of flavor singlet contributions: exploiting the fact that $m_\omega, m_\phi > m_\rho$, it was demonstrated [16] that the ratio of the disconnected contribution over the total momentum-projected current-current two-point function $G(t)$, defined in Eq. (9), approaches the value $-1/9$, in the limit of large Euclidean times for $N_f = 2+1$ quark flavors. This ratio will, however, not automatically propagate into $\Pi_{\rm R}(p^2)$ that depends on $G(t)$ at all times t. Next-to-leading order chiral perturbation theory arguments show the disconnected contribution to also account for $-1/9$ of the total $\Pi_{\rm R}(p^2)$ [45]. However, this observation builds on the fact that the correlator of the isosinglet vector current $\bar{u}\gamma_\mu u + \bar{d}\gamma_\mu d$ is momentum independent to this order of chiral perturbation theory—which we found is not at all satisfied by the lattice data. Thus, direct computation of the disconnected terms cannot be avoided in a systematic study. Our numerical results will shed light onto the size of the disconnected contribution at low p^2.

III. VACUUM POLARIZATION FROM SUSCEPTIBILITIES

A. The method

The photon vacuum polarization tensor (1) can also be interpreted as a momentum space current-current correlation function

$$\Pi_{\mu\nu}(p) = \frac{1}{V_4}\langle \tilde{j}_\mu(p)\tilde{j}_\nu(-p)\rangle, \tag{11}$$

where V_4 denotes the four-dimensional volume of the system and $\tilde{j}_\mu$ is the Fourier transform of the electromagnetic current defined in Eq. (2):

$$\tilde{j}_\mu(p) = \int \mathrm{d}^4x e^{ipx} j_\mu(x). \tag{12}$$

Depending on the lattice definition of j_μ, the polarization tensor (11) may or may not renormalize multiplicatively with Z_V^2. Here, we work with a conserved current, i.e. $Z_V = 1$.

In the following we relate the vacuum polarization to the leading response of the free energy density f of the system to background electromagnetic fields. To illustrate the relation between the two objects on a qualitative level, it is instructive to represent the vacuum polarization tensor by the diagram

where a momentum p flows in and out of the photon legs. Here, the gray blob indicates all possible closed loops formed by quark and gluon propagators—i.e. the perturbative expression for the free energy density f. The legs may be thought of as photons corresponding to a background electromagnetic field A_μ with momentum p. Pulling out these legs is achieved by taking appropriate derivatives of f with respect to the background field. While background electric fields turn the Euclidean QCD action complex and are thus problematic in lattice simulations, background magnetic fields can be realized without complications. Employing the latter gives access to the spatial components Π_{ij} and hence to all components $\Pi_{\mu\nu}$ since in Euclidean spacetime at zero temperature the indices can be relabeled at will.

To find the background field corresponding to $\Pi_{\mu\nu}(p)$, we define the magnetic fields

$$\mathbf{B}^p(x) = B\sin(px)\mathbf{e}_3, \qquad \mathbf{B}^0 = B\mathbf{e}_3, \tag{13}$$

pointing in the third spatial direction. While $\mathbf{B}^p$ is an oscillatory magnetic field with oscillation frequency p, $\mathbf{B}^0$ is a homogeneous background. The corresponding susceptibilities are obtained as the second derivatives of the free energy density with respect to the amplitude of the magnetic field:

$$\chi_p = -\left.\frac{\partial^2 f[\mathbf{B}^p]}{\partial(eB)^2}\right|_{B=0}. \tag{14}$$

These susceptibilities are normalized by the square of the elementary charge $e > 0$ to ensure that only the renormalization group-invariant combination eB appears in the definitions. Note that χ_p can be evaluated on gauge ensembles generated at $B = 0$.

The explicit calculation in Appendix A shows that

$$2\chi_p = \Pi(p^2), \qquad \chi_0 = \Pi(0). \tag{15}$$

These relations form a new representation of the vacuum polarization function in terms of susceptibilities with respect to the magnetic fields defined in Eq. (13) and are the main result of this article.

Unlike the conventional method, where the polarization function is extracted from the same set of position space current-current correlators for all momenta, Eq. (15) gives access to $\Pi(p^2)$ at one single lattice momentum p. While this certainly increases the costs of calculating Π over a large range of momenta, it also allows for a better signal-to-noise ratio within momentum regions of particular interest. As argued above, for the determination of the hadronic contribution to the muon anomalous magnetic moment $a_\mu^{\rm had,LO}$, low momenta $p^2 \sim 0.03$ GeV^2 are much more important than the high-p region. While $\langle j_\mu(x) j_\nu(0)\rangle$ mixes information about all allowed values of p, here such a mixing is avoided.

Just like the vacuum polarization tensor, χ_p and χ_0 can also be separated into connected and disconnected contributions. We demonstrate in Sec. IV below that, using this new approach, an unprecedented accuracy can be achieved for both the connected and the disconnected contributions to the vacuum polarization function, already at moderate computational costs. An additional advantage of the method is that it gives direct access to $\Pi(0)$.

To summarize, to arrive at a prediction for $a_\mu^{\mathrm{had,LO}}$ it is desirable to improve the accuracy in the low-p region and to calculate $\Pi(0)$ independently. The method we propose accomplishes both of these requirements.

B. Renormalization

Before presenting the details of the implementation and our numerical results, it is instructive to discuss the renormalization properties of χ_0 in more detail. Equation (15) reveals that the homogeneous susceptibility is additively divergent, just as $\Pi(0)$. To see where this divergence comes from, let us consider the multiplicative renormalization of the background magnetic field (and the corresponding renormalization of the electric charge),

$$e^2 = Z_e^{-1} e_r^2, \qquad B^2 = Z_e B_r^2, \qquad eB = e_r B_r, \tag{16}$$

with the renormalization factor

$$Z_e = 1 + 2b_1 e_r^2 \log(\mu a), \tag{17}$$

where a is the lattice spacing (inverse of the regulator) and μ the renormalization scale. Notice that since the magnetic field is external and has no dynamics, only the lowest-order QED β-function coefficient—denoted as b_1—appears in Z_e [46–48].

The total free energy density f^{tot} of the system is the sum of f and the energy $B^2/2$ of the magnetic field. Since varying the background field should not change the ultraviolet properties of the system, f^{tot} must be free of B-dependent divergences. This implies that the divergence of the pure magnetic energy

$$\frac{B^2}{2} = \frac{B_r^2}{2} + b_1 (eB)^2 \log(\mu a) \tag{18}$$

is exactly canceled by an analogous divergence of f. Plugging this divergence into the definition (14), we obtain

$$\chi_0 = 2b_1(a) \log(\mu a). \tag{19}$$

The renormalization scale μ is fixed by the requirement that there should be no finite quadratic terms in f^{tot} other than $B_r^2/2$ [46]. Let us emphasize that b_1 is the lowest-order coefficient of the QED β function, however, with all QCD corrections taken into account. To highlight this, we explicitly indicate the dependence of b_1 on the lattice spacing. Perturbatively, this reads [49]

$$b_1(a) = \sum_{f=u,d,s} (q_f/e)^2 \frac{1}{4\pi^2} \left[1 + \frac{g^2(a)}{4\pi^2} + \cdots \right], \tag{20}$$

where $g^2(a)$ is the QCD coupling. Equation (19) allows us to connect lattice results for χ_0 to perturbation theory, once the lattice spacing is small enough, cf. Ref. [48].

C. Implication for hot or dense QCD

As a side remark, we mention that the correspondence (15) can be generalized to high temperatures. In this case it results in a relation between the entropy density and the perturbative Adler function [48]. The latter is defined as the logarithmic derivative of the polarization function with respect to the squared momentum [26]:

$$D(p^2) = 12\pi^2 \frac{\partial \Pi(p^2)}{\partial \log(p^2)}. \tag{21}$$

Let us consider QCD at a high temperature T, which exceeds all other dimensionful scales in the system. In this limit, the argument of Π is set by a thermal scale $\mu_{\mathrm{th}} = 2\pi T$, leading to the correspondence $\Pi(\mu_{\mathrm{th}}^2) \leftrightarrow \chi_0(T^2)$. (The susceptibility at high temperatures indeed only depends on T^2 [48].) For the Adler function, this implies the relation

$$D(\mu_{\mathrm{th}}^2) \longleftrightarrow 12\pi^2 \frac{\partial \chi_0}{\partial \log T^2} = 6\pi^2 T \frac{\partial^2 s}{\partial (eB)^2}\bigg|_{B=0}, \tag{22}$$

where in the second step we used the definition of the entropy density $s \equiv -\partial f/\partial T$. Equation (22) reveals that the leading dependence of the entropy density on the magnetic field at high temperatures is fixed by the Adler function, i.e. by perturbative QED physics. Repeating the above argument with T replaced by a chemical potential μ (or by an isospin chemical potential μ_{I}) gives an analogous relation for the quark number density $n = -\partial f/\partial \mu$ at high μ (or for the isospin density $n_{\mathrm{I}} = -\partial f/\partial \mu_{\mathrm{I}}$ at high μ_{I}). We believe these are highly nontrivial findings.

IV. SIMULATION DETAILS AND NUMERICAL RESULTS

We employ the $N_f = 2+1$ staggered lattice ensembles [50,51] generated at physical pion and kaon masses. Each ensemble—summarized in Table I—consists of a hundred to a few hundred effectively statistically decorrelated configurations. Details of the simulation algorithm and of the lattice setup can be found in Refs. [50,52,53].

A. Oscillatory susceptibilities

First we discuss results on the susceptibilities $\chi_p = \Pi(p^2)/2$ with respect to the oscillatory backgrounds.

TABLE I. Lattice ensembles investigated; the largest lattice spacing reads $a_0 = 0.29$ fm.

N_s	N_t	β	a [fm]	$\log(a/a_0)$
24	32	3.45	0.290	0
24	32	3.55	0.216	−0.295
32	48	3.67	0.153	−0.636
40	48	3.75	0.125	−0.843
40	48	3.85	0.099	−1.078

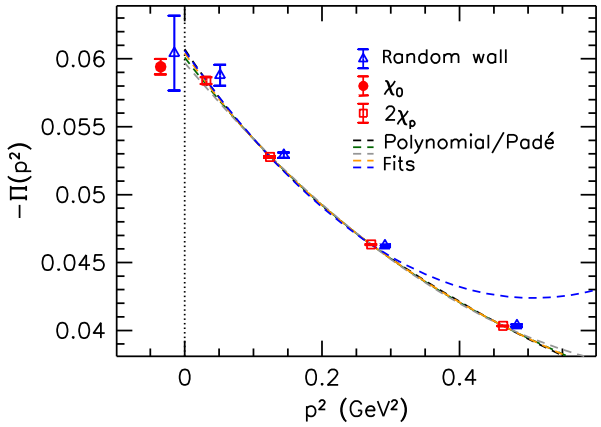

FIG. 2 (color online). The low-momentum region of the oscillatory susceptibilities as measured on the $24^3 \times 32$ configurations at $\beta = 3.45$. The curves correspond to polynomial- and Padé-type extrapolations of $2\chi_p$ to $p = 0$. The direct determination χ_0 is shifted horizontally to the left for better visibility. Also included are results obtained using random wall sources, displaced horizontally to the right.

These are determined via the noisy estimator technique described in Appendix B. A typical set of low-momentum results is shown in Fig. 2. The data include both the connected and the disconnected contributions to $\Pi(p^2)$. The figure also includes results obtained via the conventional method, however, employing stochastic wall sources (for our numerical implementation, see Appendix C). The comparison reveals full agreement between the two approaches. The statistical error of the random wall data increases towards small momenta, whereas it remains tiny even for the lowest nonvanishing p^2-value shown for the oscillatory susceptibilities. Note that the number of inversions employed to obtain the data point at the lowest momentum was the same, $N_{\rm inv} = 3000$, for both approaches.

In most previous lattice studies, $\Pi(0)$ was obtained by extrapolating $\Pi(p^2)$ to zero. Some possible extrapolations, employing polynomials or Padé approximants, fitted over various ranges in p^2, are included in the figure. These fits are also compared to the direct determinations via the homogeneous susceptibility χ_0 (see Sec. IV B below) and via the zero-momentum projected current-current correlation function $G(t)$ according to Eq. (8), again obtained using random wall sources. Within their scatter, at $p^2 = 0$ the extrapolations agree with the direct determinations. We remark that increasing the precision for the lowest few momenta stabilizes such extrapolations tremendously.

B. Homogeneous susceptibility and renormalized vacuum polarization

The susceptibility χ_0 with respect to a homogeneous background is of interest for QCD thermodynamics in magnetic fields and has been the subject of detailed studies in the past few years. The determination of χ_0 is considerably more complicated than that of χ_p due to the quantization of the magnetic flux Φ. On the one hand, oscillatory magnetic fields have zero flux and can be varied continuously, allowing for a direct differentiation with respect to B. On the other hand, homogeneous fields have nonzero flux. Therefore, such a differentiation cannot be carried out to determine χ_0; see Appendix B. Several approaches, summarized in Refs. [48,54], have been developed recently to overcome this problem. Here we compare results obtained using the finite difference method [55], the generalized integral method [48] and the half-half method [56]. The former two approaches are based on simulations at nonzero magnetic flux values, numerically differentiating the results with respect to Φ. The half-half method involves calculating expectation values directly at $B = 0$, employing a setup where the magnetic field is positive in one half and negative in the other half of the lattice. In this case, since the total flux is zero, a direct differentiation with respect to the amplitude is possible. However, the discontinuity of the magnetic field turns out to dramatically enhance finite-volume effects in χ_0; see below.[1]

In Fig. 3, we compare all three approaches. The results from the generalized integral method and from the finite difference approach are taken from Refs. [58,59] while the half-half results are new. Not all lattice spacings are covered by all the methods. While the results of the generalized integral method[2] and of the finite difference approach are consistent with each other, the half-half approach consistently underestimates the magnitude of the susceptibility. The difference between that approach on the one hand and the other two methods on the other hand is found to be as large as 10% and reduces only very slowly with increasing lattice volumes.[3] Altogether, we conclude that the half-half method is insufficient for our purposes and discard it in the following.

Perturbation theory predicts the dependence of χ_0 on the lattice spacing; see Eqs. (19)–(20). In Fig. 3 the data are plotted against $\log(a/a_0)$ to verify the expected logarithmic divergence. We include the leading $\mathcal{O}(g^2)$ QCD correction to the lowest-order QED β-function coefficient b_1. The renormalization scale μ is fitted to match the lattice results (dashed green line). In addition, we multiply the resulting

[1]These finite-volume effects cancel to a large extent in the difference $\chi_0(T) - \chi_0(T = 0)$ [57], which is relevant for QCD thermodynamics in background magnetic fields.

[2]Here we compare data obtained on $N_t > N_s$ zero-temperature lattices. On the configurations of Fef. [48] at finite (but low) temperatures, χ_0 was found to have slightly smaller absolute values for fine lattices of Table I ($\beta \geq 3.67$).

[3]The comparison between the half-half method and the generalized integral method on our coarsest lattice, already presented in Ref. [48], has been updated by increasing the statistics and the number of noisy estimators to reveal the significant difference visible in Fig. 3.

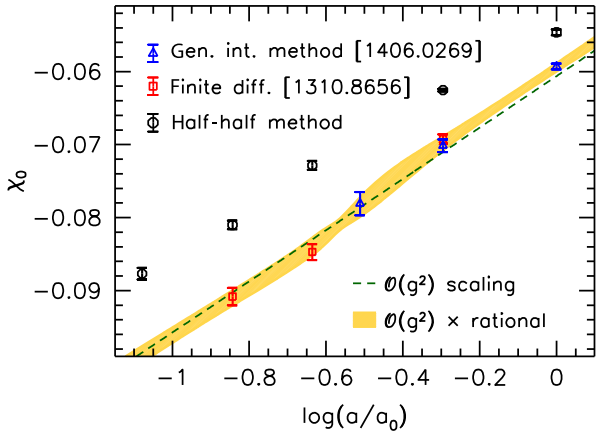

FIG. 3 (color online). Magnetic susceptibility with respect to a homogeneous background as a function of the logarithm of the lattice spacing ($a_0 = 0.29$ fm), using three different approaches (the generalized integral method [48], the finite difference method [58,59] and data generated in this study using the half-half method [56]). Also included are a comparison to $\mathcal{O}(g^2)$ perturbation theory and a parametrization via a rational *Ansatz*.

curve by a rational function that approaches unity as $a \to 0$ (solid yellow error band). This band defines the homogeneous magnetic susceptibility $\chi_0(a)$, as shown for one lattice spacing in the very left of Fig. 2. The resulting renormalization scale reads $\mu = 0.123(8)$ GeV, consistent with our determination in Ref. [48].

The $\Pi(p^2)$ results are shown for all five ensembles of Table I in Fig. 4, where $\Pi(0) = \chi_0$ with the susceptibility χ_0 determined as detailed above. Notice that the statistical uncertainties (again, both connected and disconnected terms are taken into account) within our window of lattice spacings remain at the subpercent level for $p^2 > 0$ and are about one percent for $p = 0$. Taking into account the statistical errors of $\Pi(p^2)$ and of the independently

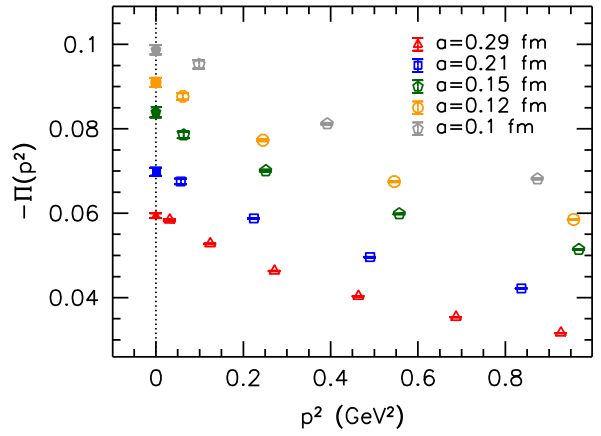

FIG. 4 (color online). Vacuum polarization via magnetic susceptibilities in the low-momentum region. The data include both connected and disconnected contributions.

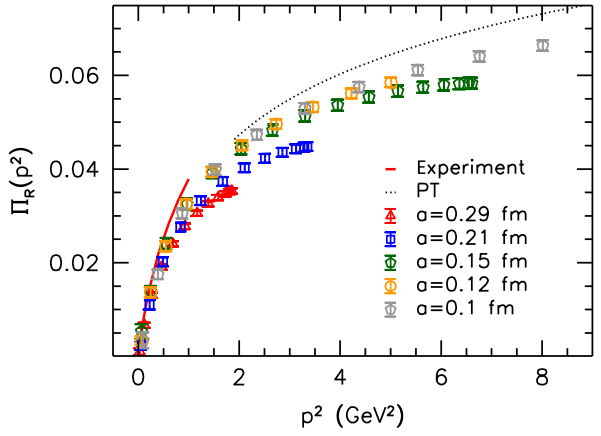

FIG. 5 (color online). Subtracted vacuum polarization with independent determinations of $\Pi(p^2)$ and $\Pi(0)$. The data include both connected and disconnected contributions. The solid red line indicates the experimental result (cf. Fig. 1) and the dotted line the three-loop perturbative prediction (see the text).

determined $\Pi(0)$, the renormalized vacuum polarization (3) is plotted in Fig. 5 for the whole momentum region under consideration. For orientation we also show the three-flavor perturbation theory result for $p^2 > 2$ GeV^2, where we truncate the formulas of Refs. [20–21] at $\mathcal{O}(\alpha_s^2)$. The perturbative curve is only defined up to an overall constant shift, which we adjust by matching to a continuum extrapolation around $p^2 = 2$ GeV^2. It is clear from the figure that—as one would expect—lattice spacing effects become more prominent towards high momenta. In addition, the vacuum polarization obtained from the experimental R ratio (cf. the blue points in Fig. 1) is included in Fig. 5.

Having obtained the renormalized hadronic vacuum polarization, we can use Eqs. (4)–(6) [13,22] to predict its contribution to the muon anomalous magnetic moment. Choosing a third-order spline interpolation, we obtain values in the range $a_\mu^{\mathrm{had,LO}} = (4\ldots5) \times 10^{-8}$ and an upward trend towards the continuum limit. This is encouraging as the R-ratio predictions of Refs. [5] and [4] for the $N_f = 2+1+1$ flavor theory read $a_\mu^{\mathrm{had,LO}} = 6.923(42) \times 10^{-8}$ and $a_\mu^{\mathrm{had,LO}} = 6.949(43) \times 10^{-8}$, respectively. However, given that the present lattices are rather coarse (0.1 fm $\lesssim a <$ 0.3 fm), we do not yet attempt a full-fledged continuum limit extrapolation. (Note that at these lattice spacings, the taste splitting of the staggered pion multiplet is still sizeable [53]. Thus, large lattice artefacts originating from the heavier pion states are not unexpected, since $a_\mu^{\mathrm{had,LO}}$ is highly sensitive to the pseudoscalar masses.)

C. Statistical accuracy and disconnected contributions

Next, we perform a quantitative comparison between the oscillatory susceptibility method, the conventional

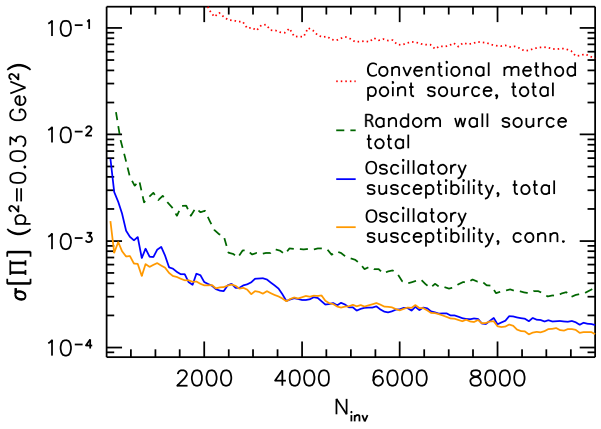

FIG. 6 (color online). Statistical error of the total (connected plus disconnected) $\Pi(p^2 = 0.03\ \mathrm{GeV}^2)$ as a function of the number of inversions. Compared are the results obtained from oscillatory susceptibilities, using point sources and random wall sources. In addition, the error of the connected oscillatory susceptibility alone is shown. Note the logarithmic scale.

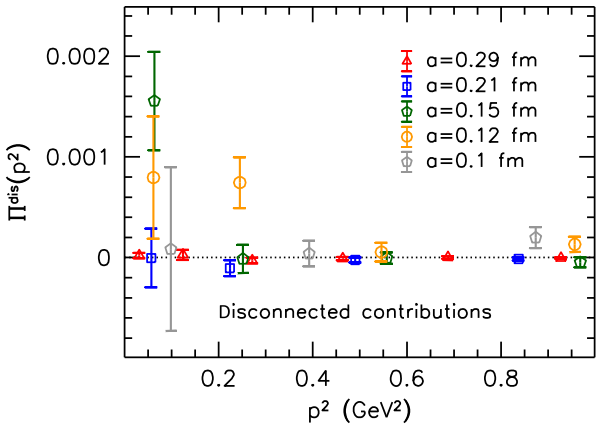

FIG. 7 (color online). Disconnected contribution to $\Pi(p^2)$ as a function of p^2 for our five lattice spacings.

approach with random wall sources and that with point sources. We demonstrate that the statistical error of $\Pi(p^2)$ can be pushed well below that of existing studies in the literature—even with the disconnected terms taken into account.

We calculated $\Pi(p^2)$ using all three methods on 120 configurations from the $\beta = 3.45$ ensemble for a single momentum $p^2 = 0.03\ \mathrm{GeV}^2$ using an increased number of sources. Figure 6 shows the statistical error as a function of the number of inversions N_{inv}. The details of our implementation can be found in Appendixes B–C. As visible in the figure, the oscillatory susceptibility method allows us to save 50–60% of the computational effort with respect to the random wall approach. This difference mainly comes from the disconnected contributions, which can be calculated very accurately via susceptibilities. In fact, the statistical error in this approach is dominated by the connected contribution,[4] as is also visible in the figure. As expected, the conventional method with point sources is not applicable for the determination of the disconnected terms. Obviously, it is favorable in terms of the total computer time spent to increase the number of configurations instead of the number of inversions per configuration. We remark that the total number of exact inversions necessary to achieve a given error can be considerably reduced by methods like the hopping parameter expansion [60,61], truncated eigenmode substitution [62–64], the truncated solver method [65–67] and, in the case of Wilson-like fermions, employing spin-explicit stochastic sources [68–70].

Finally, we discuss the disconnected contribution Π^{dis} in more detail. A particular feature of Π^{dis} is that it requires no additive renormalization. To see this, note that $\Pi^{\mathrm{dis}}(0)$ vanishes in the perturbative continuum limit, since it is of order $g^6(a)$ in the strong coupling [21], which dampens the logarithmic divergence and results in $\Pi^{\mathrm{dis}}(0)$ to fall off as $1/\log^2(a)$ for $a \to 0$. In our three-flavor case the disconnected term even vanishes identically in perturbation theory due to $\sum_{f=u,d,s} q_f = 0$, once quark masses can be neglected, i.e. $a^{-1} \gg m_s$. Based on this observation, in Fig. 7 we plot the unsubtracted disconnected vacuum polarization for all our lattice spacings. (The number of inversions was $N_{\mathrm{inv}} = 800$ for each momentum, with the exception of the leftmost point.) Overall, Π^{dis} is consistent with zero, where the two points that deviate by more than two standard deviations from this assumption are statistically expected and no systematic dependence on the lattice spacing or on the volume is apparent. With the exception of three outliers with large error bars, all central values are below 2×10^{-4} in magnitude.

Using all available estimators ($N_{\mathrm{inv}} = 20000$) for the $\beta = 3.45$ ensemble at $p^2 = 0.03\ \mathrm{GeV}^2$, our most accurate determinations for the unsubtracted and the subtracted vacuum polarizations read

$$\begin{aligned} p^2 = 0.03\ \mathrm{GeV}^2\colon\ \Pi &= -0.058362(117), \\ \Pi^{\mathrm{dis}} &= +0.000021(026), \\ \Pi_{\mathrm{R}} &= +0.002355(198). \end{aligned} \tag{23}$$

Here, $\Pi(p^2)$ and $\Pi^{\mathrm{dis}}(p^2)$ were measured using the oscillatory susceptibility method. (We highlight again that the error of Π^{dis} is much smaller than that of the total Π.) The vacuum polarization at zero momentum was obtained via random wall sources. Based on the discussion above

[4]To see why this is the case, note that the number of estimates increases quadratically with N_{inv} for the disconnected terms but only linearly for the connected ones; see the discussion in Appendix B. Therefore, the error on the latter eventually overtakes that of the former, before both show the expected asymptotic $\sigma^2 \simeq c_1(1 + c_2/N_{\mathrm{inv}})$ falloff. The inherent gauge noise c_1 can only be reduced by increasing the number of configurations.

about the vanishing of $\Pi^{\mathrm{dis}}(0)$ in the continuum limit, only the connected part of $\Pi(0)$ is necessary for the subtraction. The relative error of the so-obtained Π_{R} at this momentum is 8%, and is dominated by the error of $\Pi(0)$. Clearly, towards higher p^2, where the magnitude of $\Pi(p^2)$ increases, the relative error on Π_{R} rapidly decreases.

V. SUMMARY

We developed a new approach to determine the hadronic vacuum polarization $\Pi(p^2)$ on the lattice. It is based on calculating magnetic susceptibilities χ_p with respect to oscillatory background fields for $p^2 > 0$ and a homogeneous background for $p^2 = 0$. The proof of the equivalence between χ_p and $\Pi(p^2)$ is given in Appendix A. The oscillatory susceptibilities are obtained by evaluating the appropriate expectation values using noisy estimators, as described in Appendix B. Unlike the conventionally used approach, based on position space current-current correlators, which mix information about all possible lattice momenta, the present method enables us to determine the vacuum polarization with increased precision for individual low momenta. The low-momentum region is of relevance for an accurate determination of the leading hadronic contribution to the muon anomalous magnetic moment. In principle, the lattice determination of $\Pi(p^2) - \Pi(0)$ at a selected set of low momenta can also be combined with experimental results for the R ratio to increase the accuracy of $a_\mu^{\mathrm{had,LO}}$.

The proposed method not only reduces statistical errors at low momenta but also allows for an independent measurement of $\Pi(0)$, instead of having to rely on extrapolations of $\Pi(p^2)$ from $p^2 > 0$. We discussed three different methods to determine the homogeneous susceptibility $\chi_0 = \Pi(0)$. The most straightforward method, which relies only on simulations at zero magnetic field (the so-called half-half method), was found to suffer from large finite-volume effects of up to 10% of the full value. Instead, we combined existing results on χ_0 from Refs. [48,58] that are based on simulations at nonzero background fields. We also tested stochastic wall sources to obtain $\Pi(0)$ as the second moment of a momentum projected current-current correlation function and found that it can compete with the accuracy of the homogeneous susceptibility for a sufficiently large number of random sources. It is interesting to note that χ_0 can also be obtained via stochastic wall sources at finite temperatures, giving direct access to the renormalized magnetic susceptibility $\chi_0(T) - \chi_0(T = 0)$ that enters the QCD equation of state at finite magnetic fields [48,55,56,58,71,72].

The method was tested on staggered $N_f = 2 + 1$ flavor ensembles with various lattice spacings. Already on a few hundred configurations, a statistical accuracy below one percent is achieved for $\Pi(p^2)$. The disconnected contributions have been included in all cases. Figure 8 shows an order-of-magnitude comparison of our statistical accuracy to that of existing calculations in the literature, wherever data or figures with error bars are available for Π at $p^2 \approx 0.03$ GeV^2 [17,24,27,30–35,41]. [Note that the approach followed in Ref. [36] involves parametrizing the lattice data for the zero-momentum projected two-point function $G(t)$ of Eq. (9), making a comparison for Π difficult.] We remark that this incomplete comparison does not distinguish between different lattice volumes, spacings or pion masses but just serves as a qualitative indicator of the accuracy. It reveals that our statistical errors, obtained on a comparably small number of gauge configurations, are by far the smallest within the lattice studies shown in Fig. 8. However, the approach of employing the experimental R ratio is still by about an order of magnitude more accurate. Nevertheless, by applying the methods used in this paper to ensembles with substantially higher statistics, the desired accuracy may be reached in the near future.

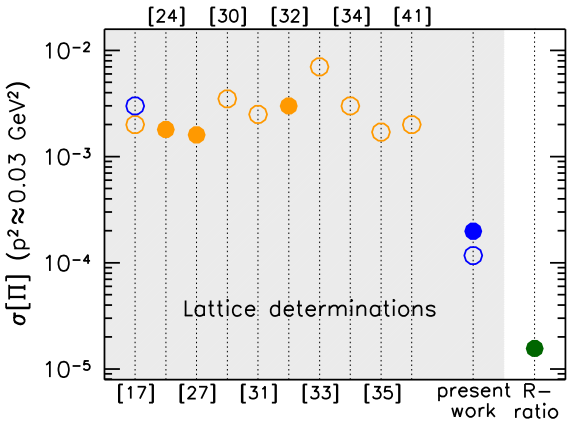

FIG. 8 (color online). The statistical error of the vacuum polarization at low momenta around $p^2 = 0.03$ GeV^2 for several lattice studies in the literature and for the present work (shaded area). Open points denote the error of the unsubtracted $\Pi(p^2)$, while full symbols indicate that of the renormalized $\Pi_{\mathrm{R}}(p^2)$. Studies involving only the connected contribution are indicated in yellow, while those also taking into account the disconnected terms are indicated in blue. The determination using the experimental R ratio is also included for comparison (solid green point).

ACKNOWLEDGMENTS

This research was funded by the Deutsche Forschungsgemeinschaft (DFG) (Grant No. SFB/TRR 55). The authors acknowledge useful discussions with Bastian Brandt, Vladimir Braun, Falk Bruckmann, Pavel Buividovic, Andreas Schäfer, Kálmán Szabó and in particular with Bogdan Malaescu and Andreas Hoecker who made available to us preliminary results on the renormalized hadronic vacuum polarization function obtained from their analysis of R-ratio measurements.

APPENDIX A: PROOF OF EQ. (15)

Below we prove the main result of the paper, Eq. (15). We define the free energy density $f=-\log\mathcal{Z}/V_4$, in terms of the partition function $\mathcal{Z}$ of the system in a four-dimensional volume V_4. $\mathcal{Z}$ is obtained evaluating the Euclidean functional integral over the gluon, quark and antiquark fields $\mathcal{A}_\mu$, ψ_f and $\bar\psi_f$,

$$\mathcal{Z}=\int\mathcal{D}\mathcal{A}_\mu\prod_{f=1}^{N_f}\mathcal{D}\bar\psi_f\mathcal{D}\psi_f e^{-S},\qquad S=\int \mathrm{d}^4x\mathcal{L},\tag{A1}$$

where the action S is the integral of the Lagrange density $\mathcal{L}$. Without loss of generality, the magnetic field of Eq. (13) is chosen to point in the third spatial direction and is generated by a vector potential $\mathbf{A}^p=\mathbf{B}^p$:

$$A_2^p=\int \mathrm{d}x_1 B^p,\qquad A_0^p=A_1^p=A_3^p=0.\tag{A2}$$

Here the superscript p indicates the oscillation frequency of the magnetic field, cf. Eq. (13). The vector potential enters the Lagrange density via minimal coupling:

$$\begin{aligned}\mathcal{L}&=\mathcal{L}_g+\sum_{f=1}^{N_f}\bar\psi_f(\not{D}_f^p+m_f)\psi_f,\\ \not{D}_f^p&=\gamma_\mu(\partial_\mu+i\mathcal{A}_\mu+iq_fA_\mu^p),\end{aligned}\tag{A3}$$

where $\mathcal{L}_g$ is the gluonic Lagrangian and m_f denote the quark masses.

In Eq. (A2) we chose a gauge, in which the photon vector potential only couples to the second component j_2 of the electromagnetic current. Therefore, this background probes the $\Pi_{22}(p)$ entry of the vacuum polarization tensor, where we orient the momentum p to point in the x-direction: $p=(p_1,0,0,0)$. In this case, employing Eq. (1), the vacuum polarization (11) simplifies to

$$\Pi_{22}(p)=\frac{1}{V_4}\langle\tilde j_2(p)\tilde j_2(-p)\rangle=-p_1^2\Pi(p^2).\tag{A4}$$

For reasons that will become clear in a moment, we consider two different oscillatory background fields

$$B^{\sin,p}(x)=B\sin(px),\qquad B^{\cos,p}(x)=B\cos(px),\tag{A5}$$

and denote the corresponding susceptibilities accordingly as $\chi_p^{\sin}$ and $\chi_p^{\cos}$.

Integrating the Lagrange density (A3) and going to momentum space, the magnetic field-dependent part S_B of the action reads

$$\begin{aligned}S_B(B^0)&=B\tilde j_2'(0),\\ S_B(B^{\cos,p})&=B[\tilde j_2(p)-\tilde j_2(-p)]/(2p_1),\\ S_B(B^{\sin,p})&=B[\tilde j_2(p)+\tilde j_2(-p)]/(2ip_1),\end{aligned}\tag{A6}$$

where the prime denotes differentiation with respect to p_1. Inserting these expressions into the partition function (A1) and differentiating twice with respect to eB in order to obtain the susceptibilities (14) results in

$$\begin{aligned}\chi_0&=\frac{1}{V_4}\langle\tilde j_2'(0)\tilde j_2'(0)\rangle,\\ \chi_p^{\cos}&=\frac{1}{V_4}\frac{1}{4p_1^2}\langle[\tilde j_2(p)-\tilde j_2(-p)]^2\rangle,\\ \chi_p^{\sin}&=-\frac{1}{V_4}\frac{1}{4p_1^2}\langle[\tilde j_2(p)+\tilde j_2(-p)]^2\rangle.\end{aligned}\tag{A7}$$

Note that terms containing the squares of expectation values, e.g., $\langle\tilde j_2'(0)\rangle^2$ for χ_0, vanish due to parity symmetry $B\leftrightarrow -B$ and thus do not appear in Eq. (A7).

Comparing Eqs. (A4) and (A7) shows that

$$\chi_p^{\cos}+\chi_p^{\sin}=\Pi(p^2).\tag{A8}$$

In the zero-momentum limit, the oscillatory magnetic fields satisfy

$$\lim_{p\to0}B^{\cos,p}=B^0,\qquad \lim_{p\to0}B^{\sin,p}=0,\tag{A9}$$

which, together with Eq. (A8), implies for the homogeneous case

$$\chi_0=\Pi(0).\tag{A10}$$

Furthermore, the cos- and sin-type magnetic fields only differ in a phase and are equivalent due to translational invariance. Therefore, the two oscillatory susceptibilities coincide, giving

$$2\chi_p=\Pi(p^2).\tag{A11}$$

Note that the equivalence of $\chi_p^{\sin}$ and $\chi_p^{\cos}$ only holds for nonzero momenta and breaks down at $p=0$. In addition, on the periodic lattice the two oscillatory susceptibilities differ at the maximal momentum $p_{\max}=\pi/a$ where the cos-type vector potential becomes zero on all lattice sites and thus $\chi_{p_{\max}}^{\cos}$ vanishes identically. [Still, Eq. (A8) holds even at this momentum.]

Relations (A10)–(A11) represent the basis of our analysis to obtain the vacuum polarization function from magnetic susceptibilities. We remark that implementing Eqs. (A2), (A4) and (A9) may be thought of as using δ-sources in momentum rather than in position space when computing $\Pi(p^2)$. A similar idea to relate hadronic matrix elements to the response to background fields was also discussed in Ref. [73].

APPENDIX B: IMPLEMENTATION OF THE SUSCEPTIBILITIES

In this appendix we present the details of the lattice computation of the susceptibilities (14). First of all we have to address the implications of magnetic flux quantization.

In a finite periodic volume, the magnetic flux Φ through the perpendicular plane $L_1 \times L_2$ (the magnetic field is oriented in the third spatial direction) is quantized [74],

$$\Phi = \int \mathrm{d}x_1 \mathrm{d}x_2 eB = 6\pi N_b, \qquad N_b \in \mathbb{Z}, \tag{B1}$$

where we exploited that the smallest electric charge in the system equals $q_d = -e/3$. Thus, flux quantization prohibits direct differentiation with respect to the amplitude of the magnetic field, unless the flux identically vanishes. For the oscillatory field $B^p(x)$ of Eq. (13) this is indeed the case, making the differentiation with respect to B straightforward. For the homogeneous background, the flux is nonzero and, thus, B becomes a discrete variable. Various methods to calculate χ_0 are summarized in Refs. [48,54].

After integrating out the quark fields, the lattice partition function becomes an integral over the gluonic links $U_\mu \approx e^{ia\mathcal{A}_\mu}$:

$$\mathcal{Z} = \int \mathcal{D}U_\mu e^{-S_g} \prod_{f=1}^{N_f} (\det M_f^p)^{\frac{1}{4}}, \quad M_f^p = \not{D}_f^p + m_f. \tag{B2}$$

Here we employed (rooted) staggered quarks to discretize the fermion matrix M_f^p, but the method trivially generalizes to different discretizations. The U(1) vector potential of Eqs. (A2)–(A3) enters M_f^p via the substitution

$$U_2(x_1) \mapsto U_2(x_1) \cdot e^{iaq_f A_2^p} = U_2(x_1) \cdot e^{iaq_f B \frac{\sin(px)}{p_1}}, \tag{B3}$$

where in the second step we inserted the vector potential for the cos-type magnetic field with momentum p_1 in the first spatial direction. The improvement $p_1 \mapsto \hat{p}_1$ is carried out in the denominator of the exponent, similarly as in the conventional approach, cf. Eq. (10). The derivative with respect to B is then obtained as

$$\chi_p = \frac{1}{V_4}\left\langle \mathcal{C}_p^2 + \frac{\partial \mathcal{C}_p}{\partial(eB)} \right\rangle, \tag{B4}$$

where

$$\mathcal{C}_p = \frac{1}{4}\sum_f \frac{q_f}{e} \mathrm{tr}[(M_f^p)^{-1}\dot{M}_f^p], \tag{B5}$$

and the dot denotes differentiation with respect to the combination $q_f B$ at $B = 0$. Having taken the derivative at $B = 0$, we can exploit the equality of the up and down quark matrices $M_u = M_d \equiv M_\ell$ due to the coincident light quark masses. Then the susceptibility reads (suppressing the index p and using the electric charge values $q_u/2 = -q_d = -q_s = e/3$)

$$\begin{aligned}\chi_p = {} & \frac{1}{4V_4}\left\langle \frac{5}{9}\mathrm{tr}(M_\ell^{-1}\ddot{M}_\ell - M_\ell^{-1}\dot{M}_\ell M_\ell^{-1}\dot{M}_\ell) + \frac{1}{9}\mathrm{tr}(M_s^{-1}\ddot{M}_s - M_s^{-1}\dot{M}_s M_s^{-1}\dot{M}_s)\right\rangle \\ & + \frac{1}{16V_4}\left\langle \frac{1}{9}\mathrm{tr}(M_\ell^{-1}\dot{M}_\ell)\mathrm{tr}(M_\ell^{-1}\dot{M}_\ell) + \frac{1}{9}\mathrm{tr}(M_s^{-1}\dot{M}_s)\mathrm{tr}(M_s^{-1}\dot{M}_s) - \frac{2}{9}\mathrm{tr}(M_\ell^{-1}\dot{M}_\ell)\mathrm{tr}(M_s^{-1}\dot{M}_s)\right\rangle, \end{aligned} \tag{B6}$$

where, like in Eq. (B5), the prefactors $1/4$ and $1/16$ are due to the use of rooted staggered fermions.

The first expectation value on the right-hand side is the connected contribution, whereas the second one is the disconnected term. The traces are measured via a set of noisy estimators ξ_j, $j = 1 \ldots N_\xi$. Taking into account the cyclicity of the trace, the total number of necessary inversions is $4N_\xi$ (twice for the light and twice for the strange quark matrix). For the calculation of N_p different momenta, some of the solutions can be recycled. This results in the total number of required inversions $N_{\mathrm{inv}} = 2N_\xi(1 + N_p)$, where the prefactor 2 again is due to $M_s^{-1} \neq M_\ell^{-1}$. We then have N_ξ independent estimates for the connected contribution. Using different stochastic sources for the strange and for the light quarks, we obtain N_ξ^2 estimates of the last disconnected term within Eq. (B6), while for the two nonflavor mixing disconnected terms we can only exploit $N_\xi(N_\xi - 1)/2$ independent variations.

APPENDIX C: IMPLEMENTATION OF RANDOM WALL SOURCES

Below we specify the details of the calculation of $\Pi(p^2)$ and of $\Pi(0)$ via stochastic wall sources. In this approach, one calculates the current-current correlator in coordinate space, and performs the Fourier transformation subsequently. Care has to be taken in defining the currents and especially their product at the same position. Usually in the literature the conserved current is considered and the contact term is subtracted in order for the lattice Ward identity (10) to hold [75]. Another possibility is to consider the product of conserved and local currents as was done in Ref. [31].

Here we demonstrate how the subtraction of the contact term can be obtained automatically if the current is defined using a background U(1) field A_μ. For simplicity, we again consider the $\mu = 2$ component of the currents and take the distance between the insertions to point in the first direction. Then we get

$$\langle j_2(x)j_2(y)\rangle = \frac{\partial^2 \log \mathcal{Z}}{\partial A_2(x)\partial A_2(y)}\bigg|_{A_2=0}$$
$$= \frac{1}{4}\left\langle \sum_f \left(\frac{q_f}{e}\right)^2 \mathrm{tr}\left[M_f^{-1}\frac{\partial^2 M_f}{\partial(q_f A_2(x))\partial(q_f A_2(y))}\delta_{x,y} - M_f^{-1}\frac{\partial M_f}{\partial(q_f A_2(x))}M_f^{-1}\frac{\partial M_f}{\partial(q_f A_2(y))}\right]\right\rangle$$
$$+\frac{1}{16}\left\langle \sum_f \frac{q_f}{e}\mathrm{tr}\left[M_f^{-1}\frac{\partial M_f}{\partial(q_f A_2(x))}\right]\right\rangle\left\langle \sum_{f'} \frac{q_{f'}}{e}\mathrm{tr}\left[M_{f'}^{-1}\frac{\partial M_{f'}}{\partial(q_{f'} A_2(y))}\right]\right\rangle. \quad \text{(C1)}$$

Notice that the first term arises due to the fact that the background field enters M_f in the exponential form $e^{iaq_f A_2}$, and it only contributes if $x = y$. Now we define

$$a^3\sum_{x_2,x_3,x_4}\frac{\partial M_f}{\partial(q_f A_2(x))} = \gamma_2\mathcal{P}_{x_1}, \qquad a^3\sum_{x_2,x_3,x_4}\frac{\partial^2 M_f}{\partial(q_f A_2(x))\partial(q_f A_2(x))} = \tau_2\mathcal{P}_{x_1}, \quad \text{(C2)}$$

where $\mathcal{P}_{x_1}$ is the projector on the slice of the lattice where the first spatial coordinate equals x_1. Here, γ_2 is the staggered discretization of the second Dirac matrix and τ_2 its equivalent with the Hermitian conjugate links multiplied by minus one,

$$\begin{matrix}(\gamma_2)_{xy}\\(\tau_2)_{xy}\end{matrix} = \frac{1}{2}[\eta_2(x)U_2(x)\delta_{y,x+a\hat{2}} \overset{+}{\underset{-}{}} \eta_2(x-a\hat{2})U_2^\dagger(x-a\hat{2})\delta_{y,x-a\hat{2}}], \quad \text{(C3)}$$

and η_μ denote the staggered phases. With these definitions we obtain for the two-point function (9), with the temporal direction replaced by the first spatial direction,

$$G(x_1-y_1) \equiv \frac{a^6}{L_2L_3L_4}\sum_{x_2,x_3,x_4}\sum_{y_2,y_4,y_4}\langle j_2(x)j_2(y)\rangle = \frac{1}{4}\left\langle \sum_f\left(\frac{q_f}{e}\right)^2 \mathrm{tr}[M_f^{-1}\delta_2\mathcal{P}_{x_1} - M_f^{-1}\gamma_2\mathcal{P}_{x_1}M_f^{-1}\gamma_2\mathcal{P}_{y_1}]\right\rangle$$
$$+\frac{1}{16}\left\langle \sum_f \frac{q_f}{e}\mathrm{tr}[M_f^{-1}\gamma_2\mathcal{P}_{x_1}]\right\rangle\left\langle \sum_{f'}\frac{q_{f'}}{e}\mathrm{tr}[M_{f'}^{-1}\gamma_2\mathcal{P}_{y_1}]\right\rangle. \quad \text{(C4)}$$

All source positions y_1 can be averaged over, keeping the distance $x_1 - y_1$ fixed, to increase statistics. Inserting the electric charges and taking into account the degeneracy of the light quark masses, this expression can be simplified, in analogy to Eq. (B6). For its evaluation we again use noisy estimators ξ_j $(j = 1\ldots N_\xi)$ that are projected using the $\mathcal{P}$ operators. One technical issue is the treatment of the second term in the connected contribution of Eq. (C4). Exploiting the η_5-Hermiticity $M_f^\dagger = \eta_5 M_f \eta_5$ of the staggered fermion matrix, the fact that $\mathcal{P}^2 = \mathcal{P}$ and that the term in question is real, we arrive at

$$\xi_j^\dagger\mathcal{P}_{y_1}\gamma_2 M_f^{-1}\mathcal{P}_{x_1}\gamma_2 M_f^{-1}\mathcal{P}_{y_1}\xi_j$$
$$= (\mathcal{P}_{x_1}\gamma_2 M_f^{-1}\mathcal{P}_{y_1}\xi_j)\cdot(\eta_5 M_f^{-1}\eta_5\gamma_2\mathcal{P}_{y_1}\xi_j)^*. \quad \text{(C5)}$$

This demonstrates how this term can be obtained for a fixed source position y_1 and any sink position x_1 using only two inversions. One of these inversions can also be reused for the calculation of the contact term involving τ_2 and for the traces in the disconnected term of Eq. (C4). The number of necessary inversions is $N_{\mathrm{inv}} = 4N_\xi$.

Putting all this together, the vacuum polarizations at finite and at zero momentum equal [cf. Eqs. (1), (8) and (10)]

$$\Pi(p^2) = -\frac{a}{\hat{p}_1^2}\sum_{x_1} e^{ip_1x_1}G(x_1),$$
$$\Pi(0) = \frac{a}{2}\sum_{x_1} f(x_1)G(x_1), \quad \text{(C6)}$$

where $\hat{p}_1 = (2/a)\sin(ap_1/2)$ is the lattice momentum and

$$f(x_1) = \begin{cases} x_1^2, & x_1 \le L_1/2, \\ (L_1-x_1)^2, & \text{otherwise}\end{cases} \quad \text{(C7)}$$

is a quadratic function consistent with the boundary conditions for a periodic lattice with linear size L_1. We mention that the separation $x - y$ of Eq. (C4) is usually chosen to lie in the temporal direction, as indicated in Eq. (8). In our setup it points in the first spatial direction to make the connection to the magnetic susceptibilities—involving x_1-dependent phases, cf. Eq. (B3)—more transparent.

[1] G. W. Bennett *et al.* (Muon g-2), Final report of the muon E821 anomalous magnetic moment measurement at BNL, Phys. Rev. D **73**, 072003 (2006).

[2] J. Grange *et al.* (Muon g-2), Muon $g-2$ technical design report, arXiv:1501.06858.

[3] T. Blum, A. Denig, I. Logashenko, E. de Rafael, B. Lee Roberts, T. Teubner, and G. Venanzoni, The muon $g-2$ theory value: present and future, arXiv:1311.2198.

[4] K. Hagiwara, R. Liao, A. D. Martin, D. Nomura, and T. Teubner, $(g-2)_\mu$ and $\alpha(M_Z^2)$ reevaluated using new precise data, J. Phys. G **38**, 085003 (2011).

[5] M. Davier, A. Hoecker, B. Malaescu, and Z. Zhang, Reevaluation of the hadronic contributions to the muon $g-2$ and to $\alpha(M_Z)$, Eur. Phys. J. C **71**, 1515 (2011).

[6] F. Jegerlehner and A. Nyffeler, The muon $g-2$, Phys. Rep. **477**, 1 (2009).

[7] M. Aoki *et al.* (E34), Report No. KEK/J-PARC, 2011.

[8] T. Aoyama, M. Hayakawa, T. Kinoshita, and M. Nio, Complete Tenth-Order QED Contribution to the Muon $g-2$, Phys. Rev. Lett. **109**, 111808 (2012).

[9] S. Moch *et al.*, High precision fundamental constants at the TeV scale, arXiv:1405.4781.

[10] M. Benayoun *et al.*, Hadronic contributions to the muon anomalous magnetic moment: strategies for the improvement of theoretical predictions and $(g-2)_\mu$: quo vadis? Workshops: mini proceedings, arXiv:1407.4021.

[11] S. Bodenstein, C. A. Dominguez, K. Schilcher, and H. Spiesberger, Hadronic contribution to the QED running coupling $\alpha(M_Z^2)$, Phys. Rev. D **86**, 093013 (2012).

[12] F. Jegerlehner, Electroweak effective couplings for future precision experiments, Nuovo Cimento **C034S1**, 31 (2011).

[13] T. Blum, Lattice Calculation of the Lowest Order Hadronic Contribution to the Muon Anomalous Magnetic Moment, Phys. Rev. Lett. **91**, 052001 (2003).

[14] M. Göckeler, R. Horsley, W. Kürzinger, D. Pleiter, P. E. L. Rakow, and G. Schierholz (QCDSF), Vacuum polarization and hadronic contribution to muon $g-2$ from lattice QCD, Nucl. Phys. **B688**, 135 (2004).

[15] Xu Feng, K. Jansen, M. Petschlies, and B. Renner, Two-Flavor QCD Correction to Lepton Magnetic Moments at Leading Order in the Electromagnetic Coupling, Phys. Rev. Lett. **107**, 081802 (2011).

[16] A. Francis, V. Gülpers, B. Jäger, H. B. Meyer, G. von Hippel, and H. Wittig, The leading disconnected contribution to the anomalous magnetic moment of the muon, *Proc. Sci.*, LATTICE2014 (2014) 128 [arXiv:1411.7592].

[17] F. Burger, G. Hotzel, K. Jansen, and M. Petschlies, Leading-order hadronic contributions to the electron and tau anomalous magnetic moments, arXiv:1501.05110.

[18] G. Martinelli, C. Pittori, C. T. Sachrajda, M. Testa, and A. Vladikas, A general method for nonperturbative renormalization of lattice operators, Nucl. Phys. **B445**, 81 (1995).

[19] M. Göckeler, R. Horsley, H. Oelrich, H. Perlt, D. Petters, P. E. L. Rakow, A. Schäfer, G. Schierholz, and A. Schiller, Nonperturbative renormalization of composite operators in lattice QCD, Nucl. Phys. **B544**, 699 (1999).

[20] P. A. Baikov, K. G. Chetyrkin, and J. H. Kühn, Adler Function, Bjorken Sum Rule, and the Crewther Relation to Order α_s^4 in a General Gauge Theory, Phys. Rev. Lett. **104**, 132004 (2010).

[21] P. A. Baikov, K. G. Chetyrkin, J. H. Kühn, and J. Rittinger, Adler function, sum rules and Crewther relation of order $O(\alpha_s^4)$: the singlet case, Phys. Lett. B **714**, 62 (2012).

[22] B. E. Lautrup, A. Peterman, and E. de Rafael, Recent developments in the comparison between theory and experiments in quantum electrodynamics, Phys. Rep. **3**, 193 (1972).

[23] C. T. Sachrajda and G. Villadoro, Twisted boundary conditions in lattice simulations, Phys. Lett. B **609**, 73 (2005).

[24] M. Della Morte, B. Jäger, A. Jüttner, and H. Wittig, Towards a precise lattice determination of the leading hadronic contribution to $(g-2)_\mu$, J. High Energy Phys. 03 (2012) 055.

[25] M. Golterman, K. Maltman, and S. Peris, New strategy for the lattice evaluation of the leading order hadronic contribution to $(g-2)_\mu$, Phys. Rev. D **90**, 074508 (2014).

[26] S. L. Adler, Some simple vacuum polarization phenomenology: $e^+e^- \to$ hadrons; the muonic atom x-ray discrepancy and $(g_\mu - 2)$, Phys. Rev. D **10**, 3714 (1974).

[27] D. Bernecker and H. B. Meyer, Vector correlators in lattice QCD: methods and applications, Eur. Phys. J. A **47**, 148 (2011).

[28] M. Benayoun, P. David, L. D. Buono, and F. Jegerlehner, An update of the HLS estimate of the muon $g-2$, Eur. Phys. J. C **73**, 2453 (2013).

[29] B. Malaescu and A. Hoecker (private communication).

[30] C. Aubin and T. Blum, Calculating the hadronic vacuum polarization and leading hadronic contribution to the muon anomalous magnetic moment with improved staggered quarks, Phys. Rev. D **75**, 114502 (2007).

[31] P. A. Boyle, L. D. Debbio, E. Kerrane, and J. M. Zanotti, Lattice determination of the hadronic contribution to the muon $g-2$ using dynamical domain wall fermions, Phys. Rev. D **85**, 074504 (2012).

[32] E. B. Gregory, Z. Fodor, C. Hoelbling, S. Krieg, L. Lellouch, H. Malak, C. McNeile, and K. K. Szabó, Leading-order hadronic contributions to $g_\mu - 2$, *Proc. Sci.*, LATTICE2013 (2014) 302 [arXiv:1311.4446].

[33] F. Burger, Xu Feng, G. Hotzel, K. Jansen, M. Petschlies, and D. B. Renner (ETM), Four-flavor leading-order hadronic contribution to the muon anomalous magnetic moment, J. High Energy Phys. 02 (2014) 099.

[34] C. Aubin, T. Blum, M. Golterman, and S. Peris, Model-independent parametrization of the hadronic vacuum polarization and $g-2$ for the muon on the lattice, Phys. Rev. D **86**, 054509 (2012).

[35] M. Marinkovic, P. Boyle, L. D. Debbio, A. Jüttner, K. Maltman, and A. Portelli, Towards the physical point hadronic vacuum polarisation from Möbius DWF, *Proc. Sci.*, LATTICE2014 (2015) 160 [arXiv:1502.05308].

[36] A. Francis, B. Jäger, H. B. Meyer, and H. Wittig, A new representation of the Adler function for lattice QCD, Phys. Rev. D **88**, 054502 (2013).

[37] R. Malak, Z. Fodor, C. Hoelbling, L. Lellouch, A. Sastre, and K. K. Szabó, Finite-volume corrections to the leading-order hadronic contribution to $g_\mu - 2$, *Proc. Sci.*, LATTICE2014 (2015) 161 [arXiv:1502.02172].

[38] G. M. de Divitiis, R. Petronzio, and N. Tantalo, On the extraction of zero-momentum form factors on the lattice, Phys. Lett. B **718**, 589 (2012).

[39] M. Göckeler, R. Horsley, W. Kürzinger, V. Linke, D. Pleiter, P. E. L. Rakow, and G. Schierholz, The vacuum polarization: power corrections beyond OPE?, Nucl. Phys. B, Proc. Suppl. **94**, 571 (2001).
[40] C. Aubin, T. Blum, M. Golterman, and S. Peris, Hadronic vacuum polarization with twisted boundary conditions, Phys. Rev. D **88**, 074505 (2013).
[41] M. Della Morte, A. Francis, G. Herdoiza, H. Horch, B. Jäger, A. Jüttner, H. B. Mayer, and H. Wittig, Study of the anomalous magnetic moment of the muon computed from the Adler function, *Proc. Sci.*, LATTICE2014 (2014) 162 [arXiv:1411.1206].
[42] C. Lehner and T. Izubuchi, Towards the large volume limit —a method for lattice QCD + QED simulations, *Proc. Sci.*, LATTICE2014 (2015) 164 [arXiv:1503.04395].
[43] Xu Feng, S. Hashimoto, G. Hotzel, K. Jansen, M. Petschlies, and D. B. Renner, Computing the hadronic vacuum polarization function by analytic continuation, Phys. Rev. D **88**, 034505 (2013).
[44] B. Chakraborty, C. T. H. Davies, G. C. Donald, R. J. Dowdall, J. Koponen, G. P. Lepage, and T. Teubner (HPQCD), Strange and charm quark contributions to the anomalous magnetic moment of the muon, Phys. Rev. D **89**, 114501 (2014).
[45] M. Della Morte and A. Jüttner, Quark disconnected diagrams in chiral perturbation theory, J. High Energy Phys. 11 (2010) 154.
[46] J. S. Schwinger, On gauge invariance and vacuum polarization, Phys. Rev. **82**, 664 (1951).
[47] G. V. Dunne, in *From Fields to Strings*, edited by M. Shifman *et al.*, Vol. 1, p. 445.
[48] G. S. Bali, F. Bruckmann, G. Endrődi, S. D. Katz, and A. Schäfer, The QCD equation of state in background magnetic fields, J. High Energy Phys. 08 (2014) 177.
[49] P. A. Baikov, K. G. Chetyrkin, J. H. Kühn, and J. Rittinger, Vector correlator in massless QCD at order $\mathcal{O}(\alpha_s^4)$ and the QED beta function at five loop, J. High Energy Phys. 07 (2012) 017.
[50] G. S. Bali, F. Bruckmann, G. Endrődi, Z. Fodor, S. Katz, S. Krieg, A. Schäfer, and K. K. Szabó, The QCD phase diagram for external magnetic fields, J. High Energy Phys. 02 (2012) 044.
[51] G. S. Bali, F. Bruckmann, G. Endrődi, Z. Fodor, S. D. Katz, and A. Schäfer, QCD quark condensate in external magnetic fields, Phys. Rev. D **86**, 071502 (2012).
[52] Y. Aoki, Z. Fodor, S. D. Katz, and K. K. Szabó, The equation of state in lattice QCD: with physical quark masses towards the continuum limit, J. High Energy Phys. 01 (2006) 089.
[53] Sz. Borsányi, G. Endrődi, Z. Fodor, A. Jakovác, S. D. Katz, S. Krieg, C. Ratti, and K. K. Szabó, The QCD equation of state with dynamical quarks, J. High Energy Phys. 11 (2010) 077.
[54] M. D'Elia, Lattice QCD with purely imaginary sources at zero and nonzero temperature, *Proc. Sci.*, LATTICE2014 (2015) 020 [arXiv:1502.06047].
[55] C. Bonati, M. D'Elia, M. Mariti, F. Negro, and F. Sanfilippo, Magnetic Susceptibility of Strongly Interacting Matter Across the Deconfinement Transition, Phys. Rev. Lett. **111**, 182001 (2013).
[56] L. Levkova and C. DeTar, Quark-Gluon Plasma in an External Magnetic Field, Phys. Rev. Lett. **112**, 012002 (2014).
[57] L Levkova (private communication).
[58] C. Bonati, M. D'Elia, M. Mariti, F. Negro, and F. Sanfilippo, Magnetic susceptibility and equation of state of $N_f = 2 + 1$ QCD with physical quark masses, Phys. Rev. D **89**, 054506 (2014).
[59] C. Bonati (private communication).
[60] C. Thron, S. J. Dong, K.-F. Liu, and H. P. Ying, Padé- Z_2 estimator of determinants, Phys. Rev. D **57**, 1642 (1998).
[61] C. Michael, M. S. Foster, and C. McNeile (UKQCD), Flavor singlet pseudoscalar and scalar mesons, Nucl. Phys. B, Proc. Suppl. **83–84**, 185 (2000).
[62] H. Neff, N. Eicker, T. Lippert, J. W. Negele, and K. Schilling, On the low fermionic eigenmode dominance in QCD on the lattice, Phys. Rev. D **64**, 114509 (2001).
[63] G. S. Bali, H. Neff, T. Düssel, T. Lippert, and K. Schilling (SESAM), Observation of string breaking in QCD, Phys. Rev. D **71**, 114513 (2005).
[64] J. Foley, J. K. Juge, A. O'Cais, M. Peardon, S. M. Ryan, and J.-I. Skullerud, Practical all-to-all propagators for lattice QCD, Comput. Phys. Commun. **172**, 145 (2005).
[65] S. Collins, G. S. Bali, and A. Schäfer, Disconnected contributions to hadronic structure: a new method for stochastic noise reduction, *Proc. Sci.*, LAT2007 (2007) 141 [arXiv:0709.3217].
[66] G. S. Bali, S. Collins, and A. Schäfer, Effective noise reduction techniques for disconnected loops in lattice QCD, Comput. Phys. Commun. **181**, 1570 (2010).
[67] T. Blum, T. Izubuchi, and E. Shintani, New class of variance-reduction techniques using lattice symmetries, Phys. Rev. D **88**, 094503 (2013).
[68] S. Bernardson, P. McCarty, and C. Thron, Monte Carlo methods for estimating linear combinations of inverse matrix entries in lattice QCD, Comput. Phys. Commun. **78**, 256 (1994).
[69] J. Viehoff, N. Eicker, S. Güsken, H. Hoeber, P. Lacock, T. Lippert, K. Schilling, A. Spitz, and P. Ueberholz (TχL), Improving stochastic estimator techniques for disconnected diagrams, Nucl. Phys. B, Proc. Suppl. **63**, 269 (1998).
[70] W. Wilcox, in *Lecture Notes in Computational Science and Engineering Vol 15: Numerical Challenges in Lattice Quantum Chromodynamics*, edited by A. Frommer *et al.* (Springer, Berlin, 2000), p. 127.
[71] G. S. Bali, F. Bruckmann, G. Endrődi, F. Gruber, and A. Schäfer, Magnetic field-induced gluonic (inverse) catalysis and pressure (an)isotropy in QCD, J. High Energy Phys. 04 (2013) 130.
[72] G. S. Bali, F. Bruckmann, G. Endrődi, and A. Schäfer, Paramagnetic Squeezing of QCD Matter, Phys. Rev. Lett. **112**, 042301 (2014).
[73] W. Detmold, Flavor singlet physics in lattice QCD with background fields, Phys. Rev. D **71**, 054506 (2005).
[74] G. 't Hooft, A property of electric and magnetic flux in nonabelian gauge theories, Nucl. Phys. **B153**, 141 (1979).
[75] L. H. Karsten and J. Smit, Lattice fermions: species doubling, chiral invariance, and the triangle anomaly, Nucl. Phys. **B183**, 103 (1981).